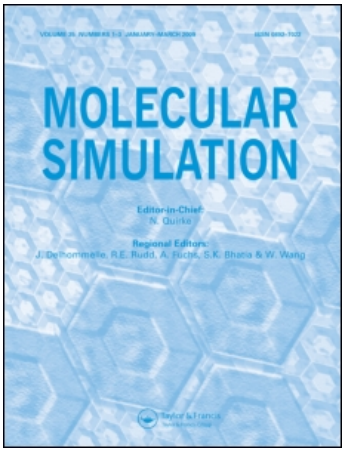

Molecular Simulation
Publication details, including instructions for authors and subscription information:
http://www.informaworld.com/smpp/title~content=t713644482

Mixing of nanofluids: molecular dynamics simulations and modelling

J. S. Hansen[a]; A. Lemarchand[a]
[a] Laboratoire de Physique Théorique de la Matiére Condensée, Université Pierre et Marie Curie, Paris Cedex 05, France

To cite this Article Hansen, J. S. and Lemarchand, A.(2006) 'Mixing of nanofluids: molecular dynamics simulations and modelling', Molecular Simulation, 32: 6, 419 — 426
To link to this Article: DOI: 10.1080/08927020600823141
URL: http://dx.doi.org/10.1080/08927020600823141

Molecular Simulation, Vol. 32, No. 6, 15 May 2006, 419–426

Taylor & Francis
Taylor & Francis Group

Mixing of nanofluids: molecular dynamics simulations and modelling

J. S. HANSEN* and A. LEMARCHAND

Laboratoire de Physique Théorique de la Matiére Condensée, Université Pierre et Marie Curie, C.N.R.S. U.M.R. 7600, 4, place Jussieu, 75252 Paris Cedex 05, France

(Received April 2006; in final form May 2006)

In this paper we study a mixing scheme, which has recently been proposed for microfluids, on the nanoscale. We do this by performing a series of nonequilibrium molecular dynamics simulations. On the nanoscale the chaotic mixing regime is captured. We discover a new phenomenon where the two mixing fluids exchange positions after leaving the mixing intersection. The results from the molecular dynamics simulations also reveal complex spatio-temporal stream velocity profiles generated by the mixing device. We find that these profiles can be modelled through an approximate analytical solution to the Navier–Stokes equation.

Keywords: Nanofluidics; Micromixing; Nonequilibrium molecular dynamics; Navier–Stokes equation

1. Introduction

In recent years a lot of attention has been paid to Micro-Electro-Mechanical Systems (MEMS) such as embedded biofluidic chips and miniaturised chemical reaction tanks [1,2,3,4,5]. In order for these devices to operate properly many issues still need to be addressed. In particular, it is not trivial to transport fluids around inside the devices. Also, reactive fluids must be brought together and mixed. This mixing could be achieved by simple diffusion, but in many practical situations the diffusion process is too slow [1] and it is therefore desirable to design a potent mixing device. Many groups have been concerned with fluid mixing. Today most of the fabricated and studied devices are, however, not applicable on very small scales since they are made of components with relatively large sizes.

A micromixing device has been developed by Lee *et al.* [6]. The device works by letting the two fluids, A and B, flow side-by-side in a main microtube. The fluids are brought into a mixing intersection, where they are perturbed by two oscillatory side flows generated by actuation channels. The two side flows are also A and B fluids. After being perturbed in the mixing intersection the two fluids are transported further downstream in the main channel and from there into the other component in the micro-electro-mechanical system. For certain operational conditions the mixer is able to perform a so-called chaotic mixing, which means that the mixing imposes an exponential growth of the interface between the two fluids. The device also exhibits a remarkable spatio-temporal resonance phenomenon. The fluid interface is highly disturbed in the mixing intersection area, but after the two fluids leave the intersection they separate again. A simple model accounts for these phenomena and are well understood at a macroscopic scale [7,8], i.e. using deterministic equations for macroscopic quantities like stream velocity. However, many questions still remain. For example is the stream velocity of the fluid in the direction of the mean flow considered to follow a parabolic expression. This is characteristic for a steady Poiseuille flow. Surely, this cannot be strictly true since the oscillatory mixing acts in the normal direction of the fluid flow. This is also pointed out in reference [7]. Moreover, while this device operates on a microscale it is uncertain whether it can be applied on even smaller scales, e.g. the nanoscale.

The purpose of this paper is two-fold: First, we wish to investigate, through nonequilibrium molecular dynamics simulations (NEMD), whether the mixing device proposed by Lee *et al.* can be applied on the nanoscale and if the spatio-temporal features can be observed on this scale. Secondly, we will use the results obtained in the

*Corresponding author. Email: schmidt@zigzak.net

Molecular Simulation
ISSN 0892-7022 print/ISSN 1029-0435 online © 2006 Taylor & Francis
http://www.tandf.co.uk/journals
DOI: 10.1080/08927020600823141

simulations to suggest an analytical model describing the stream velocity in larger detail than earlier. To accomplish this, the paper is organised as follows: In Section 2 we describe how the molecular dynamics simulations are performed and what quantities we extract from the simulations. In Section 3 we will present the results. Section 4 is devoted to elucidate the model of fluid dynamics and in Section 5 we summarise the results.

2. Molecular dynamics

A schematic diagram of the simulated system is given in figure 1. The system is composed of three different compounds A-fluid, B-fluid and wall atoms. The wall atoms are initially arranged on a face centred cubic lattice (fcc lattice) such that the geometry illustrated in figure 1 is obtained. The atoms are kept in place around their initial (or equilibrium) position through a restoring spring force $\mathbf{F}(\mathbf{r}_i) = -k(\mathbf{r}_{\text{eq}} - \mathbf{r}_i)$ where $k = 150.15\, m^2\sigma^2/\epsilon$ is the spring constant, $\mathbf{r}_i = (x_i, y_i, z_i)$ is the position of atom i and $\mathbf{r}_{\text{eq}}$ is the equilibrium position. We will explain the units below. The wall atoms and the fluid particles interact through the cut and shifted Lennard-Jones potential:

$$V(r_{ij}) = \begin{cases} 4\epsilon\left[\left(\frac{\sigma}{r_{ij}}\right)^{12} - \left(\frac{\sigma}{r_{ij}}\right)^{6}\right] - V(r_c) & \text{if} \quad r_{ij} \le r_c \\ 0 & \text{otherwise} \end{cases} \tag{1}$$

where σ and ϵ define a length scale and interaction strength, respectively, r_{ij} is the distance between particle i and j, and r_c is the cutoff radius [9,10]. The wall atoms interact with the fluid particles and the neighbouring wall atoms through equation (1) for $r_c = 2.5\sigma$ whereas $r_c = 2^{1/6}\sigma$ for the fluid–fluid interaction. The latter potential is also known as the Weeks Chandler-Anderson (WCA) potential [10]. The fluid–fluid interaction is therefore purely repulsive, whereas the fluid-wall interaction has also a distance of attraction. In this way we include a "wetting" effect between the wall atoms and the fluid particles thereby reducing the adhesive slip at the wall-fluid boundary [11]. It is worth noting that A–B interactions is the same as B–B and A–A interactions.

When the simulation begins we apply an external gravitational-like force to the fluid particles if they are located in the gravitational pressure area shown in figure 1. The force only acts in the x-direction. In order to simulate the oscillatory side flow generated by the mixing device we apply an oscillatory force to the fluid particles when they are located in one of the oscillatory pressure areas. This force acts in the y-direction. Formally, the equation of motion of fluid particle i is:

$$\frac{\mathrm{d}\mathbf{r}_i}{\mathrm{d}t} = \frac{\mathbf{p}_i}{m_i} \tag{2}$$

$$\frac{\mathrm{d}\mathbf{p}_i}{\mathrm{d}t} = \mathbf{F}_{ij} + \mathbf{i}F_g + \mathbf{j}F_o, \tag{3}$$

where $\mathbf{p}_i$ is the momentum vector, m_i the mass, $\mathbf{F}_{ij} = -\operatorname{grad} V(r_{ij})$, $\mathbf{i}$ and $\mathbf{j}$ are the usual unit vectors in $\mathbf{R}^3$. F_g and F_o are the applied gravitational force and oscillatory

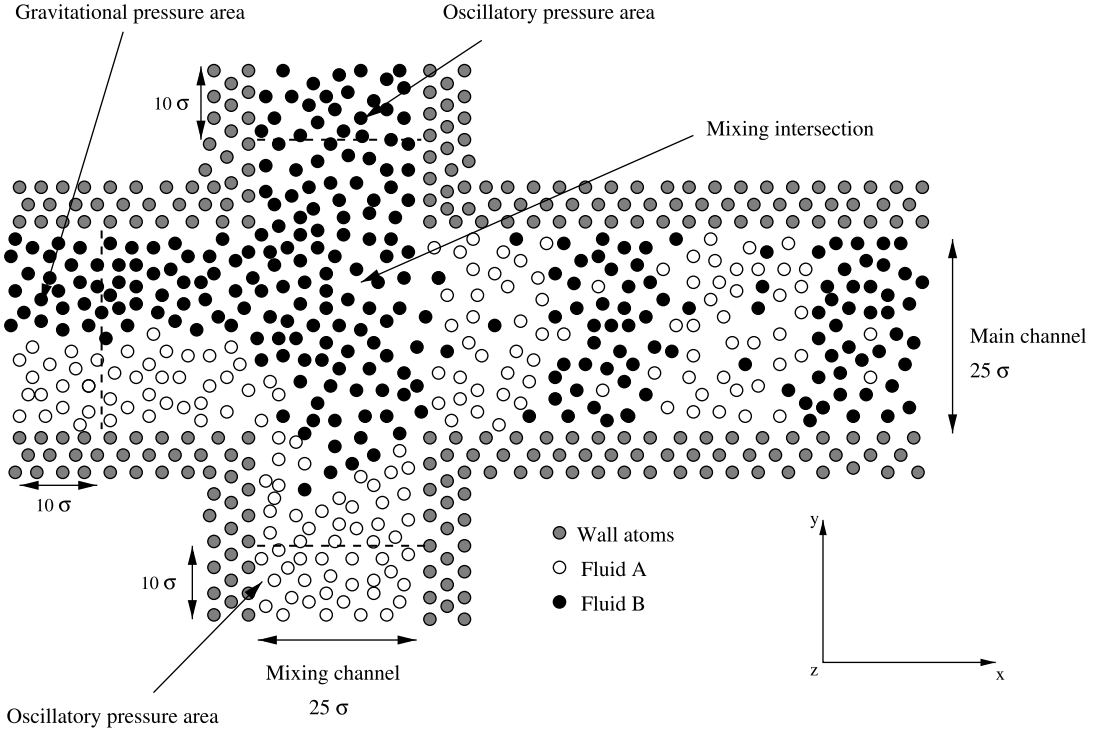

Figure 1. Schematic illustration of the system in the x–y plane. The system dimension is in all simulations: $L_x \times L_y \times L_z = 132.0\sigma \times 58.1\sigma \times 8.4\sigma$. The main channel and mixing channel have a width of $l = 25\sigma$.

force, that are respectively given by:

$$F_g = f_g \Theta(10 - x_i) \tag{4}$$

$$F_o = A \sin(\omega t)[\Theta(10 - y_i) + \Theta(y_i - L_y - 10)], \tag{5}$$

where Θ is the Heaviside step function, L_y is the length of the system in the y-direction and ω is the angular frequency of the mixing device. In all the simulations we will use $A = 0.25\ m^2\sigma^3/\epsilon$ and $f_g = 0.1\ m^2\sigma^3/\epsilon$.

We apply periodic boundary conditions in all directions. The fluid labels are changed in the gravitational pressure area such that if $y_i < L_y/2$ the label is set to A, otherwise it is set to B. If a fluid particle crosses the upper y-boundary (in the upper oscillatory pressure area) it is moved to the lower oscillatory pressure area and labeled A. On the other hand, if the particle crosses the lower y-boundary it placed in the upper oscillatory pressure area and labeled B. In all simulations the wall density is set to $0.85\ \sigma^{-3}$ and the fluid density is $0.75\ \sigma^{-3}$. The fluid particles are integrated forward in time using the leap-frog integration scheme [15]. The wall atoms are thermostated using a Nose-Hoover thermostat such that the wall temperature is $0.722\ \epsilon/k_B$ on average, where k_B is the Boltzmann constant [15,16]. The heat generated in the system due to the applied external forces is in this way removed by heat conduction at the wall-fluid boundaries. Both schemes use a time step of $h = 0.005\sigma\sqrt{m/\epsilon}$. At every time step the velocity vectors of the wall atoms are translated such that the average momentum of the wall is zero. Any physical parameter can be expressed in appropriate units of ϵ, σ and mass m. Examples, such as force and time are given above. We will here omit writing the parameters explicitly [15] for the remainder of the paper noting that all particles and atoms have the same mass, m. The method employed here is known as inhomogeneous NEMD and is described in many papers, see for example [13,12,14] and references therein.

As mentioned in the introduction our focus is to study the mixing properties of the device on the nanoscale as well as the stream velocity profiles it generates. To this end, we define the local density of A particles, as [9,12]:

$$\rho_A(r, t) = m\sum_i \delta(\mathbf{r} - \mathbf{r}_i(t)), \tag{6}$$

where δ is the Dirac delta function, and i runs over all A particles. The local stream velocity of the fluid, $\mathbf{u} = (u, v, w)$, is defined likewise:

$$\mathbf{u}(\mathbf{r}, t) = \frac{m}{\rho(\mathbf{r}, t)} \sum_i^N \mathbf{v}_i \delta(\mathbf{r} - \mathbf{r}_i(t)). \tag{7}$$

Here the index runs over all fluid particles in the system, $\mathbf{v}_i$ is the velocity vector of fluid particle i, and ρ is the local density of the fluid. To increase the signal-to-noise ratio we will present the results as an average over a time interval $\Delta t = t_2 - t_1$ and in a volume $V = \Delta x \Delta y L_z$, where L_z is the length of the system in the z-direction. The average local density can then be expressed as:

$$\bar{\rho}_A = \frac{1}{\Delta t V} \int\int_{\Delta t V} \rho_A(\mathbf{r}, t) d\mathbf{r}\, dt. \tag{8}$$

Similarly, we can define the average stream velocity $\bar{\mathbf{u}} = (\bar{u}, \bar{v}, \bar{w})$. The time interval is always $\Delta t = \pi/4\omega$ such that each mixing cycle is divided into eight equally spaced intervals. The volume element has dimensions: $V = 0.5 \times 0.5 \times L_z$. In practice the Dirac delta function is replaced by a step function which evaluates to one if fluid particle i is located in a given volume and zero otherwise. This reduces the sampling to a simple histogram method.

3. Results

Figure 2 depicts snapshots of $\bar{\rho}_A$ when the mixing device is switched off, figure 2(a), and for two different angular mixing frequencies, figure 2(b),(c). These snapshots resemble the figures given in reference [8]. It has been described earlier that the choatic mixing is characterised by a violent "folding and pushing" dynamics [7,8]. This is clearly recaptured in figure 2(c). Recall that the exponential growth in the fluid interface defines the chaotic mixing regime. In order to investigate whether this is also observed at the nanoscale we proceed the following way: In different slabs downstream from the mixing device we calculate the average number, N_{AB}, of B particles located in the first solvation shell of the A particles. We do this through the radial distribution

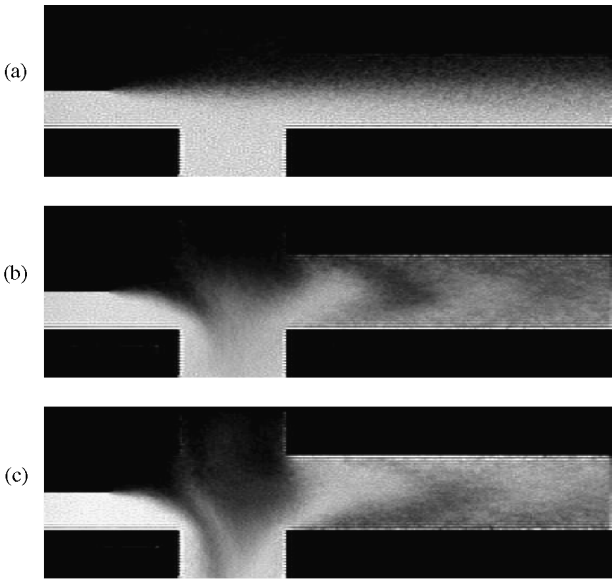

Figure 2. Snapshots of the averaged density for A particles, $\bar{\rho}_A$ Bright regions correspond to high concentration of A. (a) is when the mixing device is switched off, (b) is for $\omega = 0.074$ and (c) is for $\omega = 0.053$.

function, $g_{AB}(r)$ [9]:

$$N_{AB} = 4\pi\rho \int_0^{r'} r^2 g_{AB}(r) \mathrm{d}r \tag{9}$$

where r' is the radius of the solvation shell ($r' \approx 1.65$). In the case of chaotic mixing we will expect that the number of B particles surrounding an A particle is exponentially increasing in time. Since the fluid flows with a steady velocity N_{AB} also increases exponentially as the fluid is transported downstream from the mixing device, i.e. $N_{AB} \propto e^{\lambda x}$ where λ is the greatest Lyapunov exponent. In the situation of simple diffusion a sphere consisting of A particles has the surface area $4\pi r^2$. According to Einstein relation the mean square displacement of a particle is a linear function of time, which in turn means that the surface area of the sphere is increasing linearly in time, that is, in this case linearly with respect to x. Assuming that the number of B's in contact with this surface is proportional to the surface area the number N_{AB} is proportional to x. Surely, this is a heurestic argument that, for example, assumes that no B's penetrates the sphere and that the densities are uniform. Nevertheless, it will give an estimate of when the device is operating in the chaotic regime. Figure 3 shows $\ln(N^*_{AB})$ as a function of x in the case where $\omega = 0.053$, where we suspect the regime to be chaotic. Here $N^*_{AB} = N_{AB}(x)/N_{AB}(x = 56)$ where $N_{AB}(x = 56)$ is the number of B particles in the first solvation shell just after the mixing. The best fits to the data are also shown. It is seen that N^*_{AB} as a function of x consist of two regions of different growth. Just after the mixing intersection where $56 < x < 95$ the exponential behaviour is well captured, however, further downstream the functional behaviour is less clear. Superimposed in the figure is a plot of $\ln(N^*_{AB})$ as function of $\ln(x)$ when the mixing device is switched off. The best fit to the data yields a slope 0.75, i.e. the N_{AB} is not perfectly linear with respect to x as discussed above. It should also be noted that an exponential fit of N^*_{AB} when the mixing device is switched off gives a very poor agreement with data. We conclude that mixing can be considered as chaotic for $\omega = 0.053$.

Obtaining $\bar{\rho}_A$ we can evaluate the distribution function, p_A, that gives the probability of finding a particle A at position y, i.e. $p_A = \bar{\rho}_A(y)/\int_{-\infty}^{\infty} \bar{\rho}_A(y)\mathrm{d}y$ at some point x in the main channel. In figure 4 we present p_A at the end of the main channel for the same three parameter sets as in figure 2. When the mixing device is switched off we observe that the probability distribution is skewed right, indicating a poor mixing. The fact that there exists a mixing is simply due to the diffusion of A fluid into the region of high concentration of B fluid. The fluid structure at the fluid-wall boundary is to be expected, see for example [17]. For $\omega = 0.074$ the distribution is close to uniform in the interior of the main channel, indicating an almost perfect mixing. For lower values of the angular mixing (the chaotic regime) we see a phenomenon which to our knowledge has not been described before. The probability distribution is skewed left, meaning that fluid A and B have exchanged or swapped location. This is also indicated in figure 2(c).

The mixing scheme features resonance conditions where the two fluids are mixed at the intersection but leave it unmixed [8]. This condition is fulfilled if the time it takes the fluid to travel through the mixing intersection is an integer number times the mixing period, i.e. $n2\pi/\omega$. The average flow velocity through the main channel is measured to be 0.245. The mixing frequency has only negligible effect on this velocity. The mixing channel is $l = 25$ (figure 1), so the mean time it takes the fluid particles to cross the mixing intersection is $t \approx 102$. This in turn means that the resonance condition is fulfilled for $\omega = 0.123, 0.062$ and 0.031. In order to see whether the resonance phenomenon can be captured on nano-scale we quantify the symmetry of $p_A(y)$ by defining the second and third central moments by:

$$\mu_n = \int_{-\infty}^{\infty} (y - \mu)^n p_A(y)\mathrm{d}y \quad n = 2, 3, \tag{10}$$

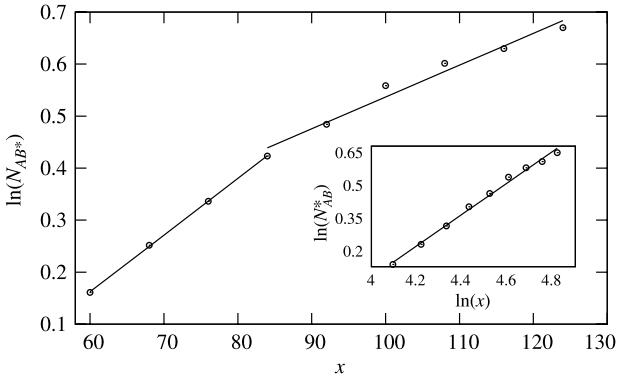

Figure 3. $\ln N^*_{AB}$ as a function of x for $\omega = 0.053$. Lines are the best fits to the data. Superimposed figure shows $\ln N^*_{AB}$ as a function of $\ln(x)$ when the mixing device is switched off. The slope is 0.75.

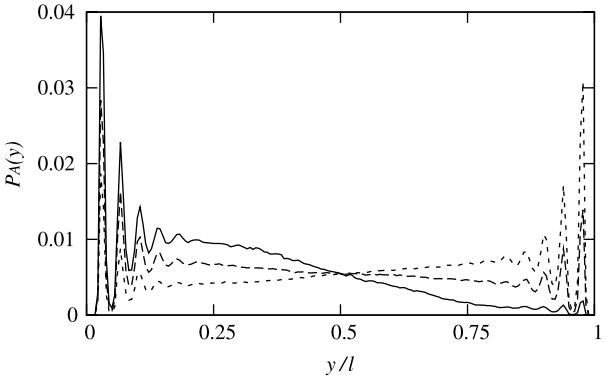

Figure 4. Probabilty functions of fluid A far downstream. Full line: the mixing device is switched off. Dashed line: $\omega = 0.074$ and dotted line is for $\omega = 0.053$. The probability functions are averaged over time and in the interval $95 < x < 105$.

where $\mu = \int_{-\infty}^{\infty} p_A(y) y \, dy$. Instead of the third central moment one usually applies the skewness $\gamma_1 = \mu_3/\mu_2^{3/2}$. As mentioned earlier, if the distribution is uniform we have perfect mixing meaning that $\gamma_1 = 0$. In the case where the mixing device is switched off the probability distribution will have a skewness $\gamma_1^d = 0.723 \pm 0.035$ due to diffusion. We now define the mixing effciency, ϵ, taking the diffusional mixing into account, as well as assuming that γ_1^d is always nonzero:

$$\epsilon = 1 - \left| \frac{\gamma_1}{\gamma_1^d} \right|. \tag{11}$$

Since $|\gamma_1^d| \geq |\gamma_1|$, the mixing effciency obeys $0 \leq \epsilon \leq 1$, where low values indicate poor mixing and high values indicate good mixing. Starting from the poor mixing region at large angular frequencies and decreasing ω, we observe in figure 5 that the mixing efficiency increases and nearly reaches 0.7 in the regime of ω that we earlier argued was the chaotic region in agreement with earlier reports. As ω decreases further the effciency drops because a phenomenon of fluid swapping: The two fluids exchange locations and the mixing becomes poor again. In the range $0.046 \leq \omega < 0.0246$ the effciency once again increases. Surely, it would be very interesting to see whether this oscillatory behavior continues, however, as the frequency decreases the computationational effort increases considerably in order to obtain acceptable signal-to-noise ratios. The three angular frequencies, $\omega = 0.123,\ 0.062,\ 0.031$, that fulfil the resonance conditions, are illustrated in figure 5 as dotted lines. When the mixing device operates at the resonance conditions the mixing effciency, ϵ, should be relative small, since the two fluids are not mixed. Whereas the nonmonotonic behavior of ϵ versus ω is well reproduced by the MD simulations, a quantitative agreement with the macrosopcic prediction for the resonant frequencies is not observed. One explanation for this can be that the resonance condition is only fulfilled for the average flow. On smale small scales microscopic fluctuations may disturb the average flow velocity considerably such that the condition is not fulfilled locally.

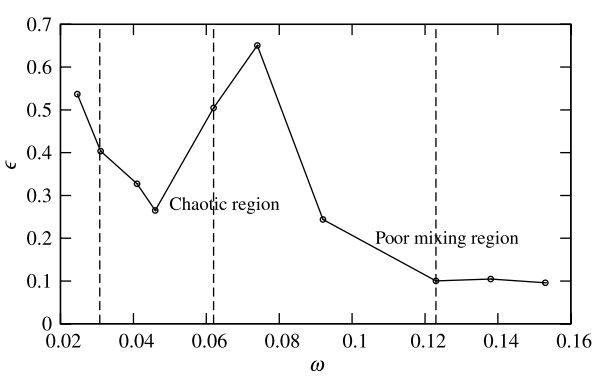

Figure 5. Mixing effciency for different mixing frequencies. The dotted lines indicate the three frequencies where the resonance condition is fulfilled. The lines are a guide to the eye.

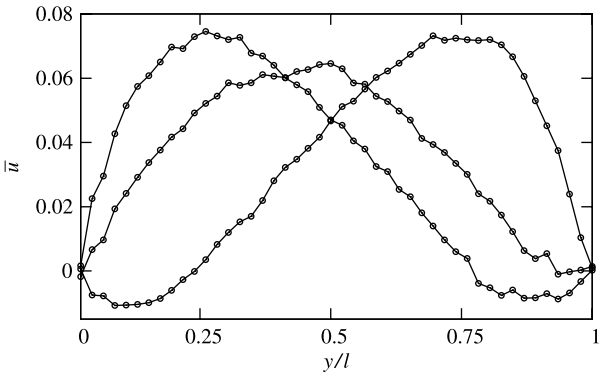

Figure 6. Velocity profiles for three different times just downstream from the mixing intersection section and for $\omega = 0.053$. The lines are a guide to the eye.

We now turn to study the stream velocity in the system. In previous studies the velocity profile in the x-direction in the main channel has been regarded as a simple parabolic function of y. This resembles a steady Poiseuille flow and as mentioned in the introduction this cannot be strictly true. This can be seen in figure 6 were we show three velocity profiles just downstream from the mixing intersection. It is seen that the stream velocity is not steady, but features spatio-temporal oscillatory dynamics. The fact that the stream velocity becomes negative is more pronounced for relatively small mixing frequencies. As we move further downstream the amplitude of the oscillations decreases and the stream velocity eventually becomes steady. The oscillations are naturally due to the perturbing side flow which acts normally to the fluid flow in the main channel. The results of the perturbations can be seen in figure 7 where the average stream velocity in the y-direction is plotted as a function of time for three different places in the main channel. It can be seen that, as the oscillatory flow generated in the mixing intersection is transported downstream by the gravitational pressure head, the amplitude decreases. We observe that the amplitude decreases linearly with x within the statistical error. Averaging over the y and z components, we may

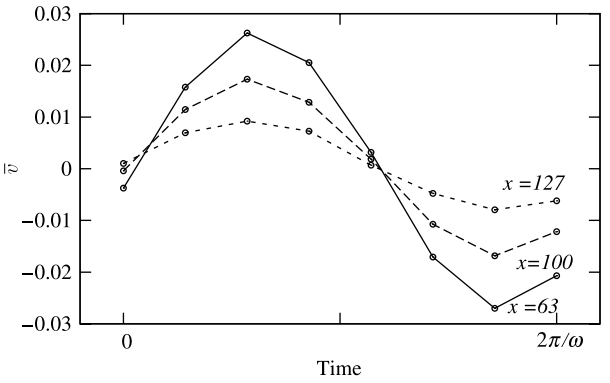

Figure 7. Averaged stream velocities, $\bar{v}$, in the y-direction in the main channel and for different values of x as a function of time for $\omega = 0.053$. The lines are a guide to the eye.

write the stream velocity in the y-direction as:

$$v(x,t) = A(x)\sin(\omega t) \tag{12}$$

where $A(x)$ is a decreasing linear function, i.e. $A(x) \to 0$ as the fluid moves downstream. Notice, that this function is closely linked to A in equation (5), but is of course not equivalent. It could now be tempting to propose a simple empirical model for $u(y, t)$ by letting a Poiseuille flow be perturbed by sinusoidal terms in y and t, e.g. at some given point x_0 in the main channel:

$$u(y,t) = \phi(y) + \mathrm{A}(x_0)\sin(\omega t)\sin(2\pi y) \tag{13}$$

$$u(y,t) = \frac{g}{2v}\left[\frac{1}{4} - \left(y - \frac{1}{2}\right)^2\right] + A(x_0)\sin(\omega t)\sin(2\pi y) \tag{14}$$

where $0 \le y \le 1$, g is the pressure gradient, v is the kinematic viscosity, and $\phi(y)$ is the parabolic expression for a Poiseuille flow. However, this equation fits very poorly with the data obtained in the molecular dynamics simulation.

4. The stream velocity

We therefore take onset in the fundamental continuity equations describing the fluid momentum [9]:

$$\rho\frac{D\mathbf{u}}{Dt} = \rho\mathbf{F}_e - \nabla\cdot p \tag{15}$$

where $D/Dt = \partial/\partial t + \mathbf{u}\cdot\nabla$ is the usual Stokes' operator, $\mathbf{F}_e$ is the external force per unit mass and $\mathbf{P}$ is the pressure tensor. If we ignore compressibility and apply Newtons law of viscosity the last term on the right-hand side is simply given by $\nabla\cdot P = -\eta\nabla^2\mathbf{u}$, where η is the shear viscosity. It is worth noting that this expression is not valid for systems where the channel width is very small, i.e. smaller than 6–7 molecular diameters [12,18]. In this case the shear viscocity varies considerably in the system and the shear viscocity may exhibit singularities and even become negative [19]. In our case, however, the main channel width is around 25 molecular diameters which is suffciently large to ignore this effect. If we furthermore ignore the z-component in the stream velocity we are led to the corresponding Navier–Stokes equation [20]:

$$\frac{\partial\mathbf{u}}{\partial t} + \mathbf{u}\cdot\nabla\mathbf{u} = \mathbf{F}_e + \nu^2\mathbf{u} \tag{16}$$

where $\mathbf{u} = (u, v)$ and $\nu = \eta/\rho$ is the kinematic viscosity. As discussed in the previous section, if we are suffciently far downstream the stream velocity is given by a Poiseuille flow, i.e. for $A(x) \to 0$, we can write $u(x, y, t) \approx \phi(y)$. As a first approach, we will therefore approximate the strain rate, that is $\partial u/\partial y$, as:

$$\frac{\partial u}{\partial y} \approx -\frac{g}{v}\left(y - \frac{1}{2}\right) \quad \text{for} \quad A(x) \to 0. \tag{17}$$

Introducing equations (12) and (17) into equation (16) and setting $\mathbf{F}_e = (g/\rho, 0)$ we have decoupled the two differential equations and obtain for u:

$$\frac{\partial u}{\partial t} - \frac{A(x)g}{v}\sin(\omega t)\left(y - \frac{1}{2}\right) = \frac{g}{\rho} + v\frac{\partial^2 u}{\partial y^2}, \tag{18}$$

such that the inertia term is an algebraic term. This nonhomogeneous parabolic differential equation is mathematical traceable if we specify the boundary and initial conditions, i.e. we write the complete problem as:

$$\frac{\partial u}{\partial t} = v\frac{\partial^2 u}{\partial y} + f(y,t), \tag{19}$$

where

$$f(y,t) = \frac{g}{\rho} + \frac{A(x)g}{v}\sin(\omega t)\left(y - \frac{1}{2}\right) \tag{20}$$

with boundary and initial conditions:

$$u(0,t) = 0, \quad u(1,t) = 0, \quad u(y,0) = \phi(y). \tag{21}$$

Note that (i) we assume non-slip conditions, (ii) start with a Poiseuillian velocity profile and (iii) the dependence on x is implicit given by $A(x)$. Moreover, it is worth noting that the model is only valid for small values of $A(x)$. The solution to the problem in equations (19)–(21) is given by the series [21]:

$$u(y,t) = \sum_{n=1}^{\infty} T_n(t)\sin(n\pi y), \tag{22}$$

at a given x and where $T_n(t)$ is a function that satisfies a more simple initial value problem. In appendix A we give a detailed mathematical treatment and simply state the solution here:

$$\begin{aligned} u(y,t) = {} & 4g\sum_{n=1,3,\ldots}\frac{1+(\rho-1)e^{-(n\pi)^2 vt}}{(n\pi)^3\rho v}\sin(n\pi y) + 2A(x)g \\ & \times\sum_{n=2,4\ldots}\frac{(n\pi)^2 v\sin(\omega t) - \omega\cos(\omega t) - \omega e^{-(n\pi)^2 vt}}{n\pi v(\omega^2 + (n\pi)^2 v)} \\ & \times\sin(n\pi y). \end{aligned} \tag{23}$$

As it can be seen is the solution divided into two contributions: The odd term contribution recaptures the Poiseuille flow, which can be seen by letting $A(x) = 0$. The even term contribution features the perturbations normal to the y-direction. As explained in Section 2, the stream velocity profiles obtained from the molecular dynamics simulations are averages over a given time interval Δt and volume V. If we neglect the variation of the stream velocity with V and only consider the asymptotic situation,

i.e. $t \to \infty$, we write the average of equation (23) as:

$$\bar{u}(y) = \frac{4g}{\Delta t}\int_{t_1}^{t_2}\left[\sum_{n=1,3\ldots}\frac{\sin(n\pi y)}{(n\pi)^3\rho\nu} + \frac{A(x)}{2} \times \sum_{n=2,4\ldots}\frac{(n\pi)^2\nu\sin(\omega t) - \omega\cos(\omega t)}{n\pi\nu(\omega^2 + (n\pi)^2\nu)}\sin(n\pi y)\right]\mathrm{d}t = \phi(y) - \frac{2gA(x)}{\Delta t} \times \left[\sum_{n=2,4\ldots}\frac{\sin(n\pi y)((n\pi)^2\nu\cos(\omega t) + \omega\sin(\omega t))}{n\pi\nu\omega((n\pi)^2\nu + \omega^2)}\right]_{t_1}^{t_2}. \quad (24)$$

In figure 8(a) we have plotted two velocity profiles obtained from the molecular dynamics simulation together with fits to equation (24) where $n \leq 10$. These profiles have been obtained just after the mixing intersection. Figure 8(b) shows the same but further down stream. We see that the analytical expression is in excellent agreement with the simulations. However, the amplitude $A(x)$ is about a factor three too large compared with the figure 7. Furthermore, it can be seen that the velocity profiles exhibits small modulations. One might argue that this is a drawback of the truncation. It is very interesting to note, however, that these modulations are also observed in NEMD simulations of Couette and Poiseuille flows for small channel widths [18,12]. It would be necessary to make very long molecular dynamics simulations in order to increase the signal-to-noise ratio and to determine if the modulations are also present at the nanoscale. It is important to stress that increasing the number of even terms in equation (24) will not lead to better agreement with the molecular dynamics results. The reason for this is that as n increases A(x) must approach the zero limit, which is not the case just after the mixing intersection.

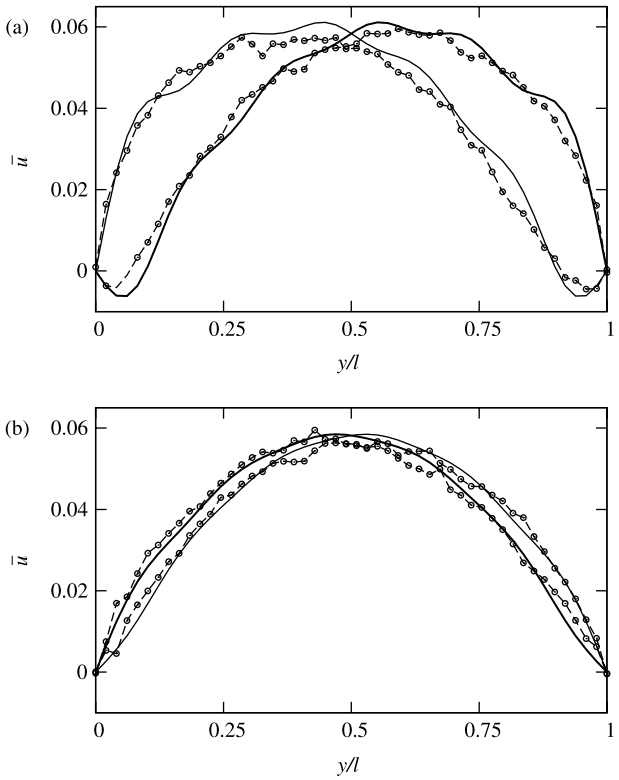

Figure 8. Stream velocity profiles obtained from the molecular dynamics (dots connected by broken lines which are a guide to the eye) and from equation (24) (full lines). $n \leq 10$ and $\omega = 0.053$. The parameters values for equation (24) are: $\nu = 1.85$; $g = 0.87$, $\rho = 0.75$. In (a) $A = 0.1$ and in (b) $A = 0.03$.

5. Conclusion

In this paper we have investigated the properties of a mixing device, recently suggested by Lee *et al.* for microfluidics, on a nanoscale. It was shown that the chaotic regime can be reached on the nanoscale. The nonmonotonic behavior of the mixing effciency versus the frequency of the oscillatory side flows is well reproduced by the molecular dynamics simulations. However the frequencies associated with the minima of the mixing effciency do not quantitatively agree with the macroscopic prediction for the resonant frequencies. We suggest that this is due to the local fluctuations which are relatively large on very small scales. In the chaotic regime we observed that the two fluids exchange location in the main channel. This has to our knowledge not been reported earlier. The molecular dynamics simulations also provided very detailed information about the stream velocity. Using these results we proposed an approximate analytical solution to the Navier–Stokes equation. The model is only valid for small oscillatory pressure gradients generated in the mixing device and gives a good agreement with the simulation results.

In this work we have considered simple miscible nonreactive fluids. In real applications the two fluids may react and the fluid may consist of complex molecules such as polymers or charged compounds. The molecular dynamics technique can also be applied in these difficult cases. However, it must be noted that the phenomena one can investigate is within the limitations of the computational power at the present day.

References

[1] T.M. Squires, S.R. Quake. Microfluidics: fluid physics at the nanoliter scale. *Rev. Mod. Phys.*, **77**, 977 (2005).
[2] N.-T. Nguyen, X. Huang. Miniature valveless pumps based on printed circuit board technique. *Sensors and Actuators A*, **88**, 104 (2000).
[3] J. Ouellette. A new wave of microfluidic devices. *Ind. Phys.*, Aug./Sept. (2003).
[4] J.C.T. Eijkel, A. van den Berg. Nanofluidics: what is it and what can we expect from it? *Microfluid. Nanofluid*, **1**, 246 (2005).
[5] P. Woais. Micropumps—summerasing the first two decades. *Microfluidics and BioMEMS*, (2001).
[6] Y.-K. Lee, C. Shih, P. Tabeling, C.M. Ho. Chaotic mixing in electrokinetically and pressure driven micro flows. *Proceedings of the MEMS*, Interlaken, Switzerland, p. 483 (2001).
[7] F. Okkels, P. Tabeling. Spatiotemporal resonance in mixing of open viscous fluids. *Phys. Rev. Let.*, **92**, 038301 (2004).
[8] A. Dodge, A. Hountondji, M.C. Jullien, P. Tabeling. Spatiotemporal resonance in a microfluidic system. *Phys. Rev. E*, **72**, 056312 (2005).

[9] D.A. Mcquarrie. *Statistical Mechanics*, Harper and Row, New York (1973).
[10] D.C. Rapaport. *The Art of Molecular Dynamics Simulations*, Cambridge University Press, Cambridge (1995).
[11] J. Castillo-Tejas, J.F.J. Alvarado, G. Gonzales-Alatorre, G. Luna-Barcenas, I.C. Sanchez, R. Macias-Salinas, O. Manero. Nonequilibrium molecular dynamics of the rheological and structural properties of linear and branched molecules. Simple shear and poiseuille ows; instabilities and slip. *J. Chem. Phys.*, **123**, 54907 (2005).
[12] K.P. Travis, B.D. Todd, D.J. Evans. Molecular spin in a fluid undergoing Poiseuille flow. *Phys. Rev. E*, **55**, 1566 (1997).
[13] J. Koplik, J.R. Banavar, J.F. Willemsen. Molecular dynamics of fluid flow at solid surfaces. *Phys. Fluids A*, **1**, 781 (1989).
[14] V.P. Stokhan, D. Nicholson, N. Quirke. Fluid flow in nanopores: an examination of hydrodynamic boundary conditions. *J. Chem. Phys.*, **115**, 3878 (2001).
[15] D. Frenkel, B. Smit. *Understanding Molecular Simulation*, Academic Press, San Diego (1996).
[16] W.G. Hoover. Canonical dynamics: equilibrium phase-space distributions. *Phys. Rev. A*, **31**, 1695 (1985).
[17] S. Toxvaerd. The structure and thermodynamics of a solid–fluid interface. *J. Chem. Phys.*, **74** (1998).
[18] I. Bitsanis, T.K. Vanderlick, M. Tirrell, H.T. Davis. Tractable molecular theory of flow in strongly inhomogeneous fluids. *J. Chem. Phys.*, **89**, 3152 (1988).
[19] J. Zhang, B.D. Todd, K.P. Travis. Viscosity of confined inhomogeneous nonequilibrium fluids. *J. Chem. Phys.*, **121**, 10778 (2004). J. Zhang, B.D. Todd, K.P. Travis. Erratum *J. Chem. Phys.* **122**, 219901 (2004).
[20] D.J. Tritton. *Physical Fluid Dynamics*, Oxford Science Publications, New York (1988).
[21] S.J. Farlow. *Partial Differential Equations for Scientists and Engineers*, Dover Edition, New York (1993).
[22] W.E. Boyce, R.C. DiPrima. *Elementary Differential Equations and Boundary Value Problems*, 6th ed., John Wiley & Sons, New York (1997).

A Solving the nonhomogeneous parabolic equation

In Section 4 we set out to solve the nonhomogeneous parabolic differential equation:

$$\frac{\partial u}{\partial t} = \nu \frac{\partial^2 u}{\partial y} + f(y,t), \tag{25}$$

where

$$f(y,t) = \frac{g}{\rho} + \frac{A(x)g}{\nu}\sin(\omega t)\left(y - \frac{1}{2}\right) \tag{26}$$

subjected to the boundary and initial conditions:

$$u(0,t) = 0, \quad u(1,t) = 0 \quad \text{and} \quad u(y,0) = \phi(y). \tag{27}$$

The solution to this problem is given by the series:

$$u(y,t) = \sum_{n=1}^{\infty} T_n(t)\sin(n\pi y). \tag{28}$$

The temporal factor $T_n(t)$ can be found through the initial value problem [21]:

$$\frac{\mathrm{d}T_n(t)}{\mathrm{d}t} + \nu(n\pi)^2 \mathrm{T}(t) = f_n(t) \quad \text{and} \tag{29}$$

$$T_n(0) = 2\int_0^1 \phi(y)\sin(ny\pi)\mathrm{d}y, \tag{30}$$

where

$$f_n(t) = 2\int_0^1 f(y,t)\sin(ny\pi)\mathrm{d}y. \tag{31}$$

For n odd:

$$f_n(t) = \frac{2A(x)g}{\nu}\sin(n\omega t)\int_0^1 \left(y - \frac{1}{2}\right)\sin(n\pi y)\mathrm{d}y + \frac{2g}{\rho}\int_0^1 \sin(n\pi y)\mathrm{d}y \tag{32}$$

$$f_n(t) = \frac{4g}{n\rho\pi} \tag{33}$$

$T_n(t)$ is then found by solving:

$$\frac{\mathrm{d}T_n(t)}{\mathrm{d}t} + (n\pi)^2 \nu \mathrm{T}(t) = \frac{4g}{n\rho\pi} \quad \text{and} \tag{34}$$

$$T_n(0) = 2\int_0^1 \phi(y)\sin(ny\pi)\mathrm{d}y = \frac{4g}{(n\pi)^3 v}. \tag{35}$$

This ordinary differential equation can be solved by standard methods [22] and the solution is:

$$T_n(t) = 4g\left[\frac{1 + (\rho - 1)e^{-(n\pi)^2 vt}}{n^3 \nu\pi\rho}\right] \quad (n \text{ odd}). \tag{36}$$

For n even:As in equation (32) we find for even n:

$$f_n(t) = -\frac{2A(x)g\sin(\omega t)}{n\pi\nu} \tag{37}$$

such that we obtain the following initial value problem:

$$\frac{\mathrm{d}T_n(t)}{\mathrm{d}t} + (n\pi)^2 \nu T = -\frac{2A(x)g\sin(\omega t)}{n\pi\nu} \quad \text{and} \tag{38}$$

$$T_n(0) = 2\int_0^1 \phi(y)\sin(ny\pi)\mathrm{d}y = \frac{4g}{(n\pi)^3 \nu}. \tag{39}$$

The solution to this problem is given by:

$$T_n(t) = \frac{2A(x)g[(n\pi)2\nu\sin(\omega \mathrm{t}) - \omega\cos(\omega t) - \omega e^{-(n\pi)^2 vt}]}{n\pi\nu(\omega^2 (n\pi)^2 \nu)} \quad (n \text{ even}). \tag{40}$$

Substituting equations (40) and (36) into equation (28) we obtain the solution given in equation (23) in Section 4.